

Received January 14, 2020, accepted February 2, 2020, date of publication February 6, 2020, date of current version February 17, 2020.

Digital Object Identifier 10.1109/ACCESS.2020.2972134

Mutual Coupling Reduction of $\pm 45^\circ$ Dual-Polarized Closely Spaced MIMO Antenna by Topology Optimization

SHUN-HUI ZHU¹, XUE-SONG YANG¹, (Member, IEEE), JIAN WANG², NIAN-SHENG NIE¹, AND BING-ZHONG WANG¹, (Senior Member, IEEE)

¹Institute of Applied Physics, University of Electronic Science and Technology of China, Chengdu 610054, China

²The 13th Research Institute of China Electronics Technology Group Corporation, Shijiazhuang 050051, China

Corresponding author: Xue-Song Yang (xsyang@uestc.edu.cn)

This work was supported by the National Natural Science Foundation of China under Grant 61731005.

ABSTRACT A hybrid topology optimization (HTO) method is adopted to reduce the mutual coupling of a $\pm 45^\circ$ dual-polarized closely spaced MIMO antenna. In order to shorten the optimization time, only the isolation structure region of the two-element MIMO antenna is selected for optimization. More importantly, by exploiting the symmetry of both the MIMO antenna and the isolation structure, only a quarter of the isolation structure needs to be optimized to achieve good antenna performance. In this way, not only the optimization variables, but also the optimization sub-objectives are greatly reduced, and the optimization time is further diminished. The performance of the dual-polarized MIMO antenna with the optimized isolation structure (OIS) is validated by both simulation and measurement. The OIS resonates in both polarizations, thus lowering the mutual coupling between co-polarization ports ($|S_{31}|$ and $|S_{42}|$) and between cross-polarization ports ($|S_{41}|$ and $|S_{32}|$) simultaneously. With the center distance of only $0.35\lambda_0$, the measured mutual coupling between different ports are reduced by 6~11 dB within the 10-dB impedance bandwidth (Reflection coefficients < -10 dB) by adding the OIS, and the highest mutual coupling between different ports is reduced from -15 to -21 dB. Besides, the antenna maintains a low profile ($0.026\lambda_0$), low cross-polarization and excellent radiation pattern performance.

INDEX TERMS Mutual coupling, dual-polarized antenna, MIMO antenna, isolation structure, hybrid topology optimization (HTO).

I. INTRODUCTION

Dual-polarized antennas have been widely used in base stations to reduce the impact of multipath fading and increase channel capacity by polarization diversity and polarization multiplexing [1]–[4]. Moreover, by using dual-polarized antennas, the number, size and overall cost of base station antennas can be greatly reduced. Multiple-input and multiple-output (MIMO) technology has grown up to be one of the crucial parts of the upcoming fifth-generation (5G) communications. There is an urgent need to design dual-polarized MIMO antennas for the 5G communications systems.

The associate editor coordinating the review of this manuscript and approving it for publication was Sotirios Goudos¹.

Due to the limited space for antenna installation, with the increase of the number of antennas, the size of antenna elements and the spacing between them must be reduced. However, reducing the element size will reduce its gain and bandwidth, which is not conducive to the channel capacity improvement. Therefore, it is better to reduce the spacing between antenna elements. When the antenna elements get closer to each other, stronger mutual coupling will be generated between antenna elements, which will seriously degrade the overall performance of the system [5]. Therefore, reducing mutual coupling between MIMO antenna elements is a significant challenge.

A variety of solutions have been suggested to reduce mutual coupling of MIMO antennas [5]–[15]. By using neutralization lines [5], electromagnetic bandgap structures [6], decoupling networks [7], resonant structures [8], etc., good

decoupling effects have been achieved for single-polarized MIMO antennas, even for those with spacing less than $0.5\lambda_0$ (λ_0 is the free space wavelength). While with the use of cutting slots [9], decoupling branches [10], baffles [11], metal cavities [12], coupled metamaterial slabs [13], resonant meta-structures [14], decoupling surfaces [15], etc., mutual coupling levels of dual-polarized MIMO antennas have been reduced. For example, in [12], a pair of metal cavities and an artificial periodic structure were utilized to reduce mutual coupling between dual-polarized antenna elements. With a center distance of $1.3\lambda_0$, mutual coupling levels between the co-polarization ports were reduced by 6~8 dB within the 10-dB impedance bandwidth (Reflection coefficients of all the ports < -10 dB). In [14], two types of resonant meta-structures were applied simultaneously to achieve the decoupling of a dual-polarized MIMO antenna. At the center distance of $0.63\lambda_0$, mutual coupling levels of both polarizations were reduced by 3~13 dB in the whole operating band. In [15], an array-antenna decoupling surface was exploited to achieve 2~11 dB mutual coupling reduction between different antenna ports with the center distance of $0.53\lambda_0$.

From the literature, there is little research on the decoupling of dual-polarized MIMO antennas with center distance less than $0.5\lambda_0$. As we know that decoupling between antenna elements is a very complex problem involving the matching, isolation, polarization purity and radiation pattern of the antenna elements. For MIMO antennas, the smaller the element spacing, the more the influence of the decoupling structure on the antenna, and the more the difficulty of its design. Accordingly, it is extremely difficult to effectively reduce mutual coupling of a dual-polarized closely spaced MIMO antenna with element spacing less than $0.5\lambda_0$.

For reducing mutual coupling of MIMO antennas, various optimization methods have also been used, including optimizing both antenna elements [16] and isolation structures [17]–[20]. In [17] and [18], fragment-type isolation structures were optimized by multi-objective evolutionary algorithm based on decomposition for single-polarized MIMO antenna and orthogonally polarized MIMO antenna. In [20], a dual-layer isolation structure was optimized for a single-polarized MIMO antenna by a hybrid topology optimization method. Except for the work in [20], in almost all the other works, only the S-parameters (return loss and isolation) of antennas were optimized, but the radiation characteristics (pattern and polarization) were not optimized simultaneously. Therefore, although the isolation performance of all the antennas was improved, the back radiation and cross-polarization characteristics of several antennas became worse.

In this work, we adopt the hybrid topology optimization (HTO) method firstly proposed in [21] to optimize a $\pm 45^\circ$ dual-polarized closely spaced MIMO patch antenna to achieve mutual coupling reduction as well as maintain good impedance matching, low cross-polarization and low back radiation. This HTO combines the scalar isotropic material with penalization (SIMP), which is a kind of material

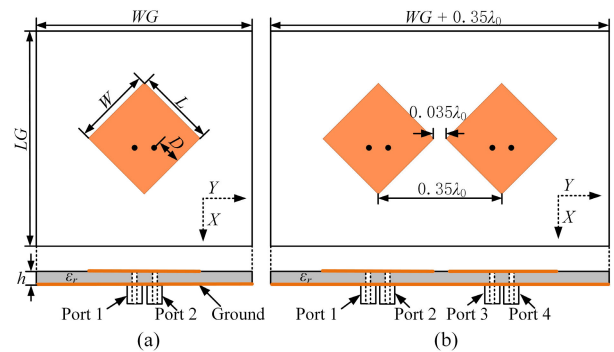


FIGURE 1. Geometries of $\pm 45^\circ$ dual-polarized antennas. (a) Single-element antenna. (b) Two-element antenna. $LG = 70$ mm, $WG = 70$ mm, $W = 25.65$ mm, $L = 25.65$ mm, $h = 3$ mm, and $D = 8.4$ mm.

distribution methods, and the level set method (LSM) [20]–[23]. In order to shorten the optimization time, only the isolation structure region of the MIMO antenna is selected for optimization. By exploiting the symmetry of both the MIMO antenna and the isolation structure, only a quarter of the isolation structure needs to be optimized. In this way, not only the optimization variables, but also the optimization sub-objectives are greatly reduced, and the optimization time is further diminished. For the dual-polarized MIMO antenna with a center distance of only $0.35\lambda_0$, owing to the topology optimization, the mutual coupling levels between different ports are reduced by 6~11 dB within the 10-dB impedance bandwidth (2.58–2.64 GHz), and the highest mutual coupling between different ports is reduced from -15 to -21 dB. Moreover, the good impedance matching, low cross-polarization, low back radiation characteristics as well as low profile of the antenna element are maintained.

II. DESIGN OF ISOLATION STRUCTURE

A. MIMO ANTENNA GEOMETRY

The microstrip patch antenna can be analyzed by the transmission line model or the cavity model. The dimensions of antenna as well as its feeding position at a specific resonance frequency can be calculated by the formula in [24]. On the basis, with a square patch, the dual-polarized antenna can be realized by using orthogonal feedings.

As shown in Fig. 1(a), a dual-polarized patch antenna is designed. The resonance frequency of the antenna is set as 2.6 GHz, one of the time division-long term evolution (TD-LTE) frequency bands and 5G frequency bands, and the structural parameters of the antenna are indicated in Fig. 1. The single-element antenna is fabricated on a square grounded F4BTM-2 substrate ($\epsilon_r = 4.4$, $\tan \delta = 0.0015$) with dimensions of $70 \times 70 \times 3$ mm³. The radiation patch with a size of 25.65×25.65 mm² is printed on the top of substrate, and it is rotated 45° relative to the substrate. The patch is fed by two coaxial probes that are located symmetrically with respect to the diagonal of the patch to excite $\pm 45^\circ$ dual-polarized electromagnetic waves.

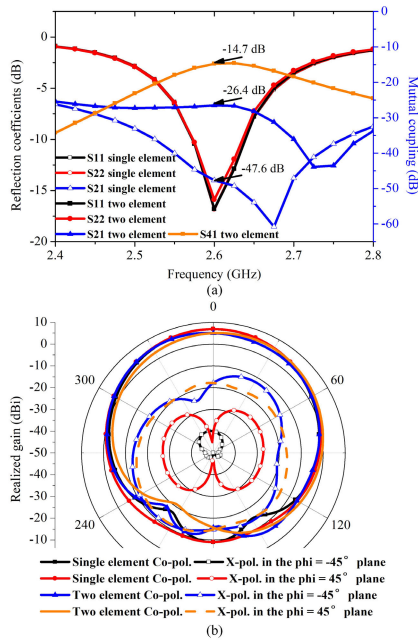


FIGURE 2. The performance of the single-element and two-element dual-polarized antennas. (a) S-parameters. (b) Radiation patterns.

TABLE 1. The performance of different antennas at 2.6 GHz.

Antenna performance	Single-element dual-polarized antenna	Two-element dual-polarized MIMO antenna	Dual-polarized antenna with XSS
$ S_{11} $ (dB)	-16.8	-16.8	-14.8
$ S_{22} $ (dB)	-16.8	-15.9	-16.1
$ S_{21} $ (dB)	-47.6	-26.4	-24.4
$ S_{31} $ (dB)	-	-15.2	-15.8
$ S_{41} $ (dB)	-	-14.7	-9.7
$ S_{32} $ (dB)	-	-14.8	-9.3
Efficiency (Port 1)	95%	89%	81%
Efficiency (Port 2)	95%	89%	81%
Gain (Port 1) (dBi)	6.9	5.0	4.0
Gain (Port 2) (dBi)	6.9	4.8	4.1
Cross-polarization level (dB)	-46.9	-22.9	-10

Based on this antenna element, a $\pm 45^\circ$ dual-polarized closely spaced two-element MIMO antenna is designed, whose dimensions are $110.3 \times 70 \times 3 \text{ mm}^3$, as shown in Fig. 1(b). The two vertices of antenna elements are very close to each other, the distance between the nearest vertices is only 4.03 mm ($0.035\lambda_0$, where λ_0 is the free-space wavelength at 2.6 GHz), and the distance between the center of two patches is only 40.3 mm ($0.35\lambda_0$).

The performance of the single-element and the two-element dual-polarized antennas is shown in Fig. 2, and that at 2.6 GHz is listed in Table 1. It can be seen that the single-element antenna has good impedance matching, low mutual coupling and low cross-polarization. In addition, the two-element antenna also has good impedance matching. However, the two-element antenna has stronger mutual

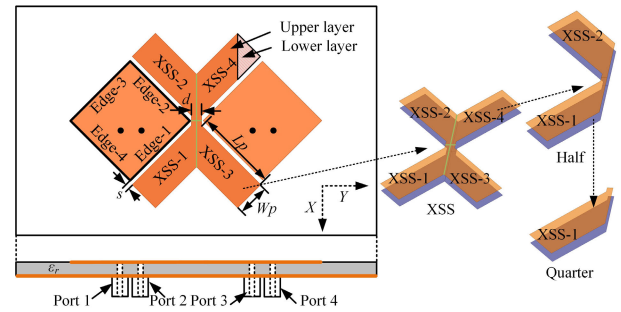


FIGURE 3. Geometry of the dual-polarized MIMO antenna with XSS. $s = 1.4 \text{ mm}$, $d = 3.18 \text{ mm}$, $W_p = 10 \text{ mm}$, $L_p = 25.53 \text{ mm}$.

coupling and higher cross-polarization under the influence of the adjacent antenna element. The cross-polarization level is increased from -46.9 dB for the single-element antenna to -22.9 dB for the two-element antenna. The mutual coupling between two ports of the same element ($|S_{21}|$) is increased from -47.6 dB for the single-element antenna to -26.4 dB for the two-element antenna. Besides, the mutual coupling between the cross-polarization ports ($|S_{41}|$) is the strongest, with a maximum of -14.7 dB . Due to the stronger mutual coupling effects, the gain and efficiency of the two-element antenna are $\sim 5.0 \text{ dB}$ and 89% , respectively, lower than those of the single-element antenna.

Adding resonant structures [8], [12], [14] or modifying ground planes [5], [9] can reduce mutual coupling. Inserting an optimized isolation structure between antenna elements, the mutual coupling between them can be reduced by generating resonance or disturbing surface current. Consequently, a two-layer symmetrical X-shaped structure (XSS) is inserted between the elements of the two-element antenna to reduce mutual coupling [6], [20], as shown in Fig. 3. The upper layer of the XSS is an X-shaped patch located at the same plane as the radiation patches, and the lower layer is an X-shaped area of the ground plane, just beneath the upper X-shaped area. The upper and lower layers have the same size, and the structural parameters are indicated in Fig. 3. The two-layer XSS can be divided into four parts, named XSS-1, XSS-2, XSS-3 and XSS-4, and they are symmetrical with respect to the X-axis and Y-axis, respectively.

The performance of the dual-polarized MIMO antenna with XSS is shown in Fig. 4, and its performance at the operating frequency of 2.6 GHz is listed in Table 1. It can be seen that the antenna has good impedance matching, but there is strong mutual coupling between the elements. The coupling between two cross-polarization ports ($|S_{32}|$) is the strongest, with a maximum of -9.3 dB . Besides, in the 0° radiation direction, the realized gain of the antenna is $\sim 4.0 \text{ dBi}$ and the cross-polarization level is -10 dB , showing low gain and poor polarization characteristics.

Next, the HTO is adopted to optimize the dual-polarized MIMO antenna with XSS to reduce mutual coupling as well as maintain good impedance matching and radiation characteristics. In order to shorten the optimization time in this

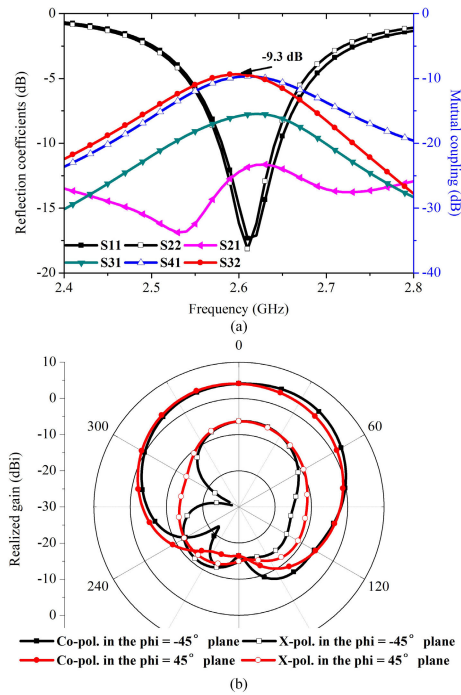


FIGURE 4. The performance of the dual-polarized MIMO antenna with XSS. (a) S-parameters. (b) Radiation patterns.

work, only the XSS region is selected for optimization, while the rest structures of the MIMO antenna are fixed. Through optimization, holes appear in the XSS region, thus changing its topology.

The symmetry of the whole antenna structure ensures that the performance of symmetrical ports is identical when excited separately. If the symmetry of the antenna can be maintained in the optimization, the number of optimization variables can be reduced by half. When one part of the XSS (e.g. XSS-1) is optimized, the other parts can be obtained according to the symmetrical relationship. Consequently, this ensures that Port 1 (Port 2) and Port 4 (Port 3) have exactly the same performance. Hence, we have the following relations:

$$|S_{11}| = |S_{44}|, \tag{1}$$

$$|S_{22}| = |S_{33}|, \tag{2}$$

$$|S_{21}| = |S_{34}|, \tag{3}$$

$$|S_{31}| = |S_{24}|. \tag{4}$$

It should be noted that, when only Port 1 is excited and all the other ports are matched, the current distribution on the feeding patch is -45° polarized, with stronger current along two edges, Edge-1 and Edge-3. Similarly, when only Port 2 is excited, the current distribution on this patch is $+45^\circ$ polarized, with stronger current along edges Edge-2 and Edge-4. Since XSS-1 is closer to Edge-1, it significantly affects the antenna performance when Port 1 is excited. Similarly, XSS-2 greatly impacts the antenna performance when Port 2 is excited. In order to ensure that XSS-1 and XSS-2 have a similar effect on the antenna when Port 1

and Port 2 are excited, respectively, XSS-1 and XSS-2 should be symmetrical. Consequently, only a quarter of the XSS should be optimized. Since the performance of antenna when Port 1 or Port 2 fed is similar, the reflection coefficients $|S_{11}|$ and $|S_{22}|$ are nearly the same, and the mutual coupling $|S_{41}|$ and $|S_{32}|$ are similar as well.

In order to reduce the numbers of optimization variables and sub-objectives, due to the symmetry of the XSS, if XSS-1 is selected for optimization, only the parameters related to Port 1 need to be optimized. To improve both the impedance matching and isolation of the antenna, the sub-objective functions contain $|S_{11}|$, $|S_{21}|$, $|S_{31}|$ and $|S_{41}|$. Meanwhile, to ensure good pattern and polarization characteristics, co-polarization and cross-polarization radiation power densities in specified angular ranges are taken as sub-objective functions as well. Besides, for suppressing the back radiation, the total radiation power density in the back direction (within a certain angular range) is taken as another sub-objective function. Consequently, a total of four S-parameters, co-polarization, cross-polarization and total radiated powers, are taken as the sub-objective functions and combined into a single objective function, as shown below

$$\begin{aligned} \min z = & w_1 \int_{\theta < \theta_1} f_{co} ds + w_2 \int_{\theta < \theta_2} f_{cx} ds + w_3 \int_{\theta > \theta_3} f_{total} ds \\ & + w_4 |S_{11}|^2 + w_5 |S_{21}|^2 + w_6 |S_{31}|^2 + w_7 |S_{41}|^2, \end{aligned} \tag{5}$$

where f_{co} , f_{cx} and f_{total} are the co-polarization, cross-polarization and total power densities of the radiated field in the far field, respectively [21]. The integral region is on the observation sphere of the far field, and θ is the zenith angle. The co-polarization field of the antenna is expected to be as high as possible in the range of $\theta_1 = 60^\circ$, and the cross-polarization field as low as possible in a wider range ($\theta_2 = 90^\circ$), while the total radiation power is suppressed in the back direction (out of the $\theta_3 = 120^\circ$ range). Besides, w_i ($i = 1, \dots, 7$) is the weighting factor, which is determined based on experimental optimizations.

B. OPTIMIZATION METHOD

The HTO method is adopted to optimize the XSS with the aim of reducing mutual coupling, while maintaining good matching and radiation characteristics of the MIMO antenna. The optimization process of the HTO in this work includes two stages, SIMP and LSM stages, similar to that in [21], and the optimization flowchart as well as the diagrams of two stages are shown in Fig. 5. The initial model is firstly optimized by the SIMP, and a rough structure with serrated boundary is obtained. Subsequently, the rough structure is further optimized by the LSM, and the final structure with smooth boundary can be obtained.

The theories of SIMP and LSM were introduced in detail in [21]. For brevity, the relevant contents won't be repeated here. As shown in Fig. 5(b), the SIMP is used to optimize the material properties in the optimization area. The optimization variable, which corresponds to the material properties of the

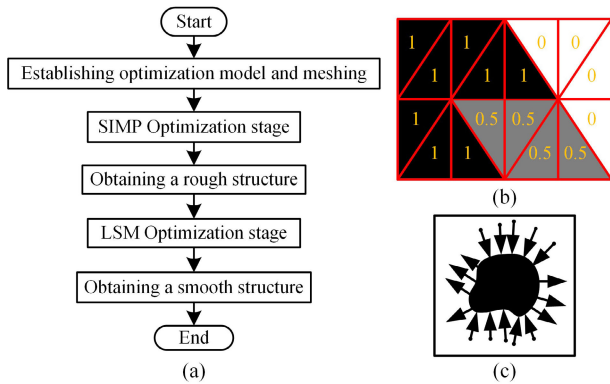


FIGURE 5. The HTO method. (a) Flowchart of the HTO process. (b) Optimization diagrams of SIMP, and (c) LSM.

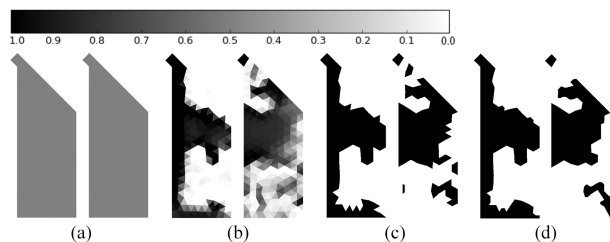


FIGURE 6. The variations of a quarter of the XSS. (a) Initial structure. (b) In the SIMP iteration. Optimized structure obtained by (c) SIMP and (d) LSM.

optimization area, can be any number between 0 and 1, where “0” stands for air (white), “1” stands for metal (black), and the number between 0 and 1 stands for lossy material (gray). At the end of optimization, all the optimization variables are either 0 or 1. In the LSM stage, the structure is optimized by varying its boundary, as shown in Fig. 5(c). The optimization variable is the position of each point on the structure boundary. Both SIMP and LSM methods are based on the gradient optimization, so the convergence rate is fast. Finally, a local optimal solution is obtained.

C. ISOLATION STRUCTURE OPTIMIZATION

In the optimization process, only a quarter of the XSS is optimized, while the rest structures of the antenna are fixed. The variations of XSS-1 are illustrated in Fig. 6. In each sub-graph, the left side shows the upper layer structure and the right side shows the lower one. In the SIMP optimization stage, the initial states of all materials in the optimization area are set as lossy materials (0.5, gray), as shown in Fig. 6(a). As the iteration proceeds, the lossy material gradually changes into air or metal, as illustrated in Fig. 6(b). Since SIMP uses a fixed mesh, a structure with rough boundary is finally obtained, as shown in Fig. 6(c).

The edge of the resulted structure is serrated, which is not conducive to fabricating and may lead to inaccurate calculation results. Therefore, LSM is further used to optimize the rough structure obtained in the first stage. In the second stage, the structure mesh is refined in each iteration. Hence, the boundary of optimized structure can be very smooth,

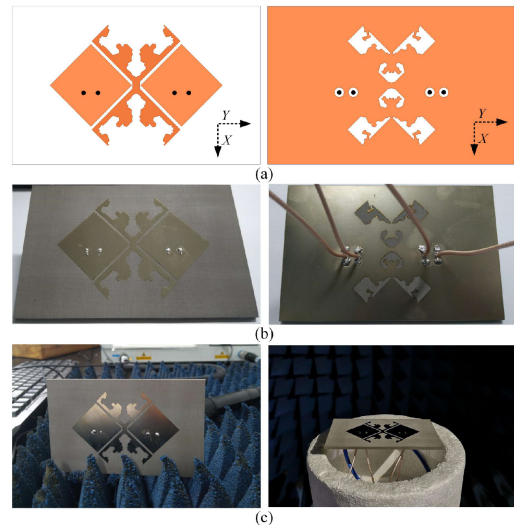


FIGURE 7. Structure of the MIMO antenna with OIS. (a) Simulation. (b) Fabrication. (c) In the test.

as depicted in Fig. 6(d), making the numerical calculation results accurate enough, and the structure easy to process.

The optimization is performed on a desktop computer with 32 GB memory and an Intel Core i7-7700 CPU at 4.2 GHz. A homemade electromagnetic simulation program that based on the finite-element method is called to evaluate the objective function. In the SIMP stage, the antenna has a total of 39867 tetrahedra meshes, and the total number of optimization variables is 2816. Each iteration takes ~ 189 seconds, and the SIMP optimization can be completed through a total of 140 iterations (~ 7.4 hours). In the LSM stage, the antenna consists of about 43000 tetrahedra meshes. Each iteration takes ~ 420 seconds, and a good optimization result can be obtained after 7 iterations (~ 0.8 hours).

III. ANTENNA RESULTS AND DISCUSSION

A. PERFORMANCE OF THE DUAL-POLARIZED MIMO ANTENNA

In the optimization process, the determination of weighting factor is very important. By adjusting weighting factors, satisfactory results can be achieved. After several experimental optimizations, an appropriate combination of weighting factors is determined. In this work, w_i ($i = 1, \dots, 7$) is finally set as $(-1, 0.5, 1, 2, 4, 4, 4)$. The final structure of the MIMO antenna with an optimized isolation structure (OIS) is shown in Fig. 7(a). In order to verify the optimization effect, the MIMO antenna with OIS is simulated, fabricated and measured. The S-parameters are measured by an Agilent E3861A vector network analyzer in an open lab environment, and the radiation patterns are measured in a SATIMO antenna measurement system in an anechoic chamber, as shown in Fig. 7(c).

The simulated (and measured) S-parameters of the MIMO antennas without and with the OIS are shown in Fig. 8, and those at the optimization frequency of 2.6 GHz are listed

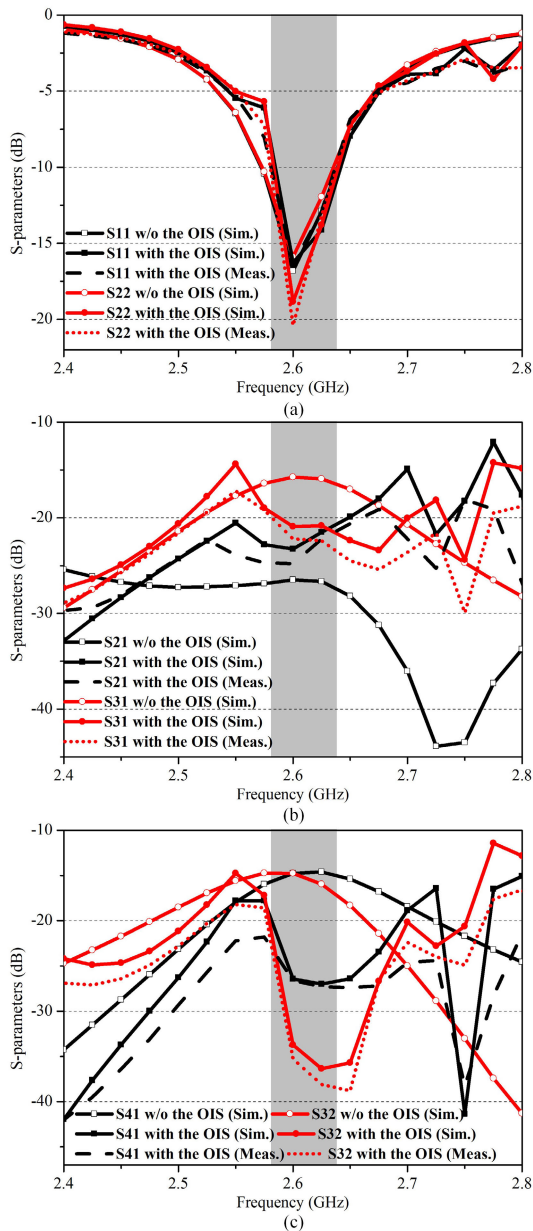


FIGURE 8. S-parameters of MIMO antennas without and with OIS. (a) $|S_{11}|$ and $|S_{22}|$. (b) $|S_{21}|$ and $|S_{31}|$. (c) $|S_{41}|$ and $|S_{32}|$.

in Table 2. From the simulated results, it can be seen that the MIMO antennas without and with the OIS have 10-dB impedance bandwidth of 2.5% (2.572–2.636 GHz) and 2.2% (2.584–2.640 GHz), respectively, and within the respective bands, the isolation is higher than 15 and 20 dB, respectively. It can be seen from Table 2, with the OIS, the simulated $|S_{11}|$ and $|S_{22}|$ at 2.6 GHz are both lower than -16 dB.

Besides, as can be seen from Fig. 8 and Table 2, for the $\pm 45^\circ$ dual-polarized MIMO antenna without OIS, the mutual coupling between cross-polarization ports ($|S_{41}|$ and $|S_{32}|$) is slightly stronger than that between co-polarization ports ($|S_{31}|$ and $|S_{42}|$). Therefore, it is more necessary to reduce the mutual coupling between

TABLE 2. The performance of different MIMO antennas at 2.6 GHz.

Antenna performance	W/o the OIS (Sim.)	With the OIS (Sim.)	With the OIS (Meas.)
$ S_{11} $ (dB)	-16.8	-16.3	-16.4
$ S_{22} $ (dB)	-15.9	-18.8	-20.4
$ S_{21} $ (dB)	-26.4	-23.2	-24.8
$ S_{31} $ (dB)	-15.2	-20.9	-22.4
$ S_{41} $ (dB)	-14.7	-26.4	-26.6
$ S_{32} $ (dB)	-14.8	-33.7	-35.3
Efficiency (Port 1)	89%	92%	83%
Efficiency (Port 2)	89%	93%	84%
Gain (Port 1) (dBi)	5.0	4.6	4.4
Gain (Port 2) (dBi)	4.8	4.9	4.5

cross-polarization ports effectively. With the OIS, the highest mutual coupling level between cross-polarization ports ($|S_{41}|$ and $|S_{32}|$) is decreased from -14.7 to -26.4 dB, and the mutual coupling between co-polarization ports ($|S_{31}|$ and $|S_{42}|$) is reduced from -15.2 to -20.9 dB. The highest simulated mutual coupling between different ports is reduced from -14.7 to -20.9 dB, witnessing a 6.2-dB reduction. However, under the influence of the adjacent antenna element and the OIS, some energy would be reflected back into the driven antenna element and absorbed by the unexcited port, so the mutual coupling between the two ports of the same element ($|S_{21}|$) is increased slightly, from -26.4 to -23.2 dB.

The measured and simulated S-parameters of the MIMO antenna with the OIS are in good agreement. Both the simulated and measured 10-dB impedance bandwidths are 2.2% (2.584–2.640 GHz and 2.581–2.637 GHz, respectively), and the simulated and measured isolation levels are higher than 20 dB and 21 dB within the respective bands, respectively.

When one port is excited and the other ports are impedance matched, the simulated (and measured) patterns of MIMO antennas without and with the OIS at 2.6 GHz are shown in Fig. 9. It can be seen that, whether Port 1 or Port 2 is excited, the patterns without and with the OIS remain essentially the same. That means the addition of the OIS neither distorts the antenna’s radiation pattern, nor generates extra back radiation.

In addition, the measured and simulated radiation patterns of the MIMO antenna with the OIS agree with each other very well. In the maximum radiation direction, the cross-polarization ratio of the antenna reaches more than 20 dB in both simulation and measurement, showing good polarization characteristics.

The efficiencies and realized gains of the MIMO antennas without and with the OIS are depicted in Fig. 10. The simulated maximum radiation efficiency with the OIS increases, and the simulated gain decreases when Port 1 is fed while increases when Port 2 is fed, as listed in Table 2. For the antenna with the OIS, the simulated/measured radiation efficiency is more than 92%/83%, and the simulated/measured realized gain in the 0° direction is greater than 4.6 dBi/4.4 dBi. Due to the materials losses and the machining

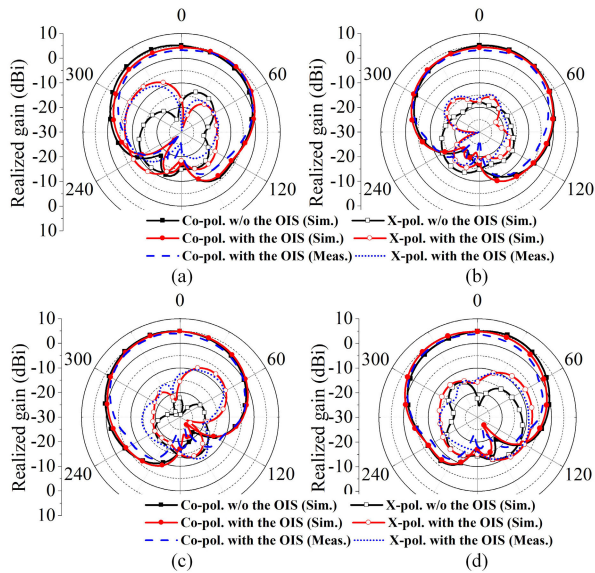


FIGURE 9. Radiation patterns of MIMO antennas without and with the OIS. (a) -45° plane and (b) 45° plane excited by Port 1. (c) -45° plane and (d) 45° plane excited by Port 2.

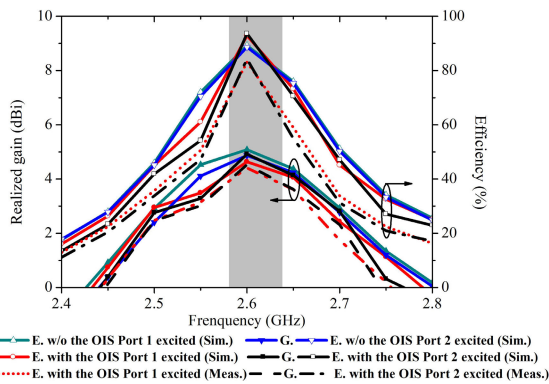


FIGURE 10. Realized gains in the 0° direction and efficiencies of MIMO antennas without and with the OIS.

and testing errors, the measured gain and efficiency of the antenna with the OIS are slightly lower than the simulated results.

Before optimization, the dual-polarized MIMO antenna with XSS has strong mutual coupling, low gain and high cross-polarization level, as shown in Table 1. After optimization, the highest mutual coupling of the dual-polarized MIMO antenna with OIS between different ports is reduced from -9 to -21 dB, the gain in the 0° radiation direction is increased from 4 to 4.9 dBi and the radiation efficiency is increased from 81% to 93%. Apparently, by using HTO to optimize the isolation structure of the dual-polarized MIMO antenna, the performance has been improved.

B. STUDY OF MUTUAL COUPLING REDUCTION

To explain the mechanism of mutual coupling reduction, the current distributions of the MIMO antennas without

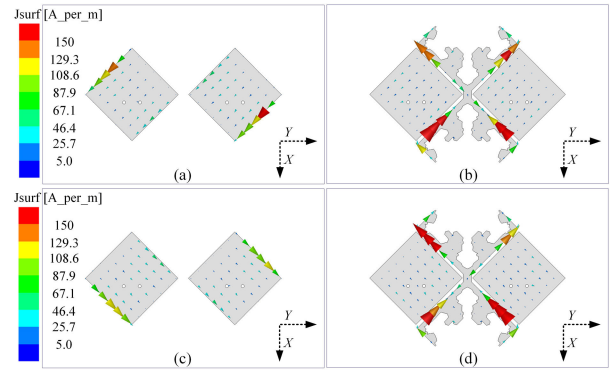


FIGURE 11. Current distributions on the patch. Excited by ports 1 and 3 (a) w/o and (b) with the OIS. Excited by ports 2 and 4 (c) w/o and (d) with the OIS.

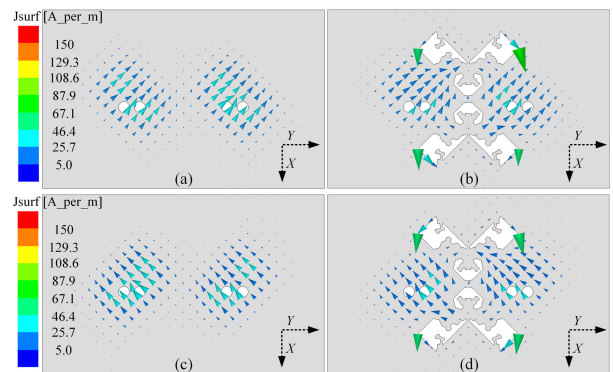


FIGURE 12. Current distributions on the ground. Excited by ports 1 and 3 (a) w/o and (b) with the OIS. Excited by ports 2 and 4 (c) w/o and (d) with the OIS.

and with the OIS are studied. The current distributions with the co-polarization ports excited are analyzed [14]. When the two co-polarization ports are excited in phase and the other two ports are terminated by $50\text{-}\Omega$ loads, the surface current distributions on the radiation patches and grounds of the antenna without and with the OIS are plotted in Figs. 11 and 12, respectively.

From Figs. 11 and 12, we can see when any two co-polarization ports are excited in phase, very strong currents are induced in the OIS area, which means, the OIS is in resonance in both polarizations. As we know, the mutual coupling between antenna elements can be availablely reduced by adding resonant structures [8], [12], [14] or modifying ground planes [5], [9]. The OIS can resonate in both polarizations, thus the mutual coupling levels between co-polarization ports ($|S_{31}|$ and $|S_{42}|$) and between cross-polarization ports ($|S_{41}|$ and $|S_{32}|$) are reduced simultaneously. Besides, the slots of the lower OIS perturb the surface current on the ground to reduce the mutual coupling. Meanwhile, adding the OIS, the surface current distribution on the radiation patch basically remains unchanged.

In addition, in order to demonstrate the mutual coupling reduction effect of the upper or lower OIS, the antenna

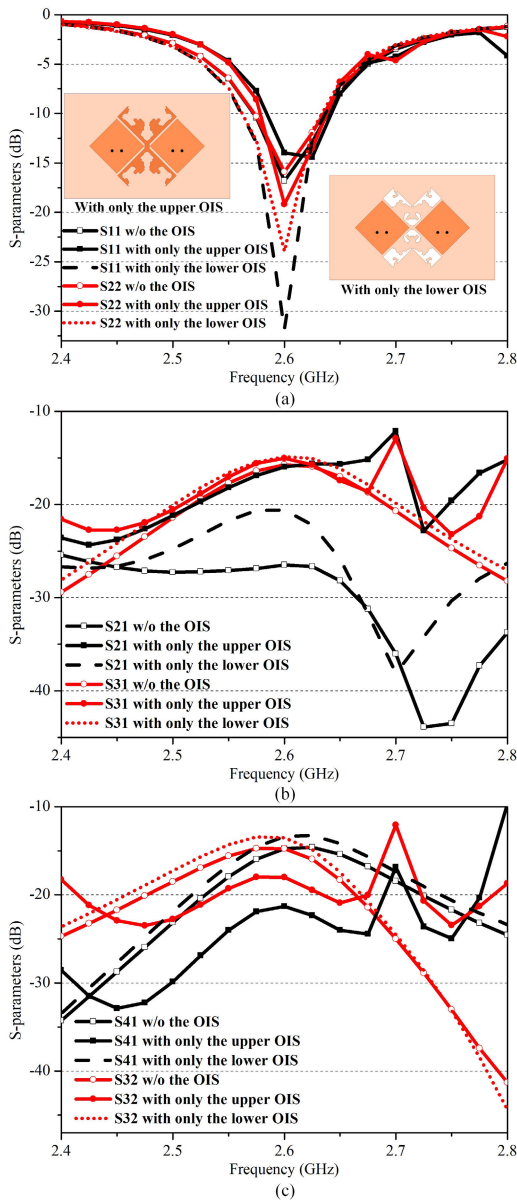


FIGURE 13. Comparison of the simulated S-parameters of the MIMO antenna without OIS, with only the upper or the lower OIS. (a) $|S_{11}|$ and $|S_{22}|$. (b) $|S_{21}|$ and $|S_{31}|$. (c) $|S_{41}|$ and $|S_{32}|$.

with only the upper or lower OIS are studied by simulation. The S-parameters of the antenna without OIS, with only the upper or lower OIS are shown in Fig. 13, and those at 2.6 GHz are indicated in Table 3. With only the upper OIS, the mutual coupling between cross-polarization ports, $|S_{41}|/|S_{32}|$, is decreased from $-14.7/-14.8$ to -21.2 dB/ -18.0 dB. Consequently, the addition of the upper OIS can reduce mutual coupling.

As shown in Table 3, with only the lower OIS, although the isolation between antenna elements is not improved, the $|S_{11}|/|S_{22}|$ is decreased from $-16.8/-15.9$ to -30.3 dB/ -23.3 dB. When with only the upper OIS, the $|S_{11}|$ is increased from -16.8 to -13.8 dB. After adding the

TABLE 3. S-parameters of different MIMO antennas (unit: dB).

S-parameters	$ S_{11} $	$ S_{22} $	$ S_{21} $	$ S_{31} $	$ S_{41} $	$ S_{32} $
Without the OIS	-16.8	-15.9	-26.4	-15.2	-14.7	-14.8
Only the upper OIS	-13.8	-19.1	-15.9	-15.3	-21.2	-18.0
Only the lower OIS	-30.3	-23.3	-20.5	-14.8	-13.3	-13.5
With the OIS	-16.3	-18.8	-23.2	-20.9	-26.4	-33.7

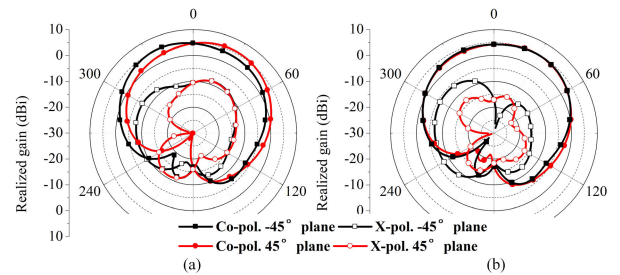


FIGURE 14. Patterns of the MIMO antenna at 2.6 GHz in the $\phi = \pm 45^\circ$ plane excited by Port 1. (a) With only the upper OIS. (b) With the entire OIS.

lower OIS, i.e., with the entire OIS, the $|S_{11}|$ is decreased from -13.8 to -16.3 dB. Therefore, the addition of the lower OIS can availably adjust matching.

Besides, the patterns of the MIMO antenna with only the upper OIS or with the entire OIS are compared in Fig. 14. It can be seen that, with only the upper OIS, the cross-polarization component of antenna will be increased. However, after adding the lower OIS, the cross-polarization component can be suppressed [19]. In a word, due to the enhanced resonance and complementary advantages of the upper and lower OIS, the mutual coupling between antenna elements is significantly reduced by the entire OIS.

C. THE RESULTS OF A LEFT-RIGHT SYMMETRICAL ISOLATION STRUCTURE

If the isolation structure to be optimized is only a left-right symmetrical structure, let's see what the optimization effect will be. As shown in Fig. 3, the XSS to be optimized is divided into the left and right parts. Next, a half of the XSS, not a quarter, is selected for the optimization. The optimization objective and process are the same as before, and the final optimized isolation structure will be a left-right symmetrical one. The MIMO antenna with the optimized left-right symmetrical isolation structure, and its S-parameters are shown in Figs. 15(a) and (b), respectively. It can be seen that optimizing only $|S_{11}|$ ($|S_{41}|$) cannot guarantee that $|S_{22}|$ ($|S_{32}|$) also has good performance. The values of $|S_{11}|$ and $|S_{22}|$, as well as $|S_{41}|$ and $|S_{32}|$ are different. Therefore, in this case, we need to optimize not only $|S_{11}|$ and $|S_{41}|$, but also $|S_{22}|$ and $|S_{32}|$, which means that, we must increase the number of optimization sub-objectives.

If the number of optimization sub-objectives is increased, the optimization time will increase accordingly. Besides, if we optimize a half instead of a quarter of the isolation structure, the optimization variables will be doubled. Apparently,

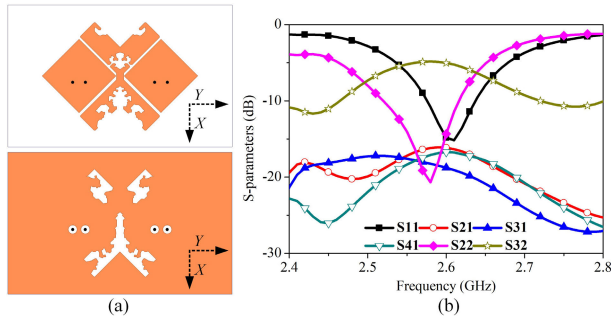


FIGURE 15. The dual-polarized MIMO antenna with only the left-right symmetrical isolation structure. (a) Geometry. (b) S-parameters.

TABLE 4. Performance of the proposed OIS and other structures.

Ref.	Technique	Center distance	Profile	Mutual coupling reduction
[9]	Cutting slots	$0.75\lambda_0/1.22\lambda_g$	$0.14\lambda_0$	7 ($ S_{21} $) dB
[10]	Decoupling branches	$0.76\lambda_0/1.59\lambda_g$	$0.067\lambda_0$	10 ($ S_{21} $) dB
[11]	Baffles	$0.58\lambda_0/1.22\lambda_g$	$0.31\lambda_0$	7 ($ S_{31} $) dB
[12]	Cavities and artificial periodic structure	$1.3\lambda_0/2.73\lambda_g$	$0.18\lambda_0$	6~8 dB
[14]	Meta-structures	$0.63\lambda_0/1.56\lambda_g$	$0.28\lambda_0$	3~13 dB
[15]	Array-antenna decoupling surface	$0.53\lambda_0/0.86\lambda_g$	$0.30\lambda_0$	2~11 dB
This work	Topology optimization	$0.35\lambda_0/0.73\lambda_g$	$0.026\lambda_0$	6~11 dB

by exploiting the symmetry of both the MIMO antenna and the isolation structure, only a quarter of the XSS is selected for optimization, the optimization time is diminished significantly. In short, for the decoupling of $\pm 45^\circ$ dual-polarized MIMO antennas, it is better to adopt an isolation structure with both left-right symmetry and up-down symmetry.

D. COMPARISON

Finally, the performance of the OIS is compared with that of the other dual-polarized MIMO antenna decoupling structures, as listed in Table 4, where λ_g is the guide wavelength in substrate. For the antennas in [9] and [10], since antenna elements are fed by a feeding network, mutual coupling between different elements does not need be considered. From the table, it is evident that, for the center distance between the antenna elements, the antenna in this work has the minimum value, only $0.35\lambda_0$ ($0.73\lambda_g$). In the case of such small element spacing, the mutual coupling between the ports of the optimized antenna is reduced by 6~11 dB, indicating that the optimized isolation structure achieves a good decoupling effect. Besides, the antenna in this work has the lowest profile and is easy to process and integrate.

IV. CONCLUSION

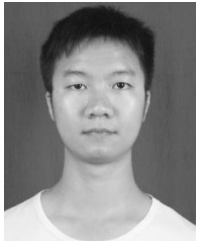
Mutual coupling of a $\pm 45^\circ$ dual-polarized closely spaced MIMO antenna has been reduced effectively by a topology optimized two-layer isolation structure. By exploiting the symmetry of the antenna and the isolation structure, the

optimization has been accelerated greatly and good optimization results have been achieved. With the optimized isolation structure, mutual coupling of the dual-polarized MIMO with a center distance of $0.35\lambda_0$ has been reduced from -15 to -21 dB at the center frequency. Besides, the antenna maintains good impedance matching, low cross-polarization and low back radiation. This method can be further applied to the optimization of Massive MIMO antennas.

REFERENCES

- [1] Q.-X. Chu, D.-L. Wen, and Y. Luo, "A broadband $\pm 45^\circ$ dual-polarized antenna with Y-shaped feeding lines," *IEEE Trans. Antennas Propag.*, vol. 63, no. 2, pp. 483–490, Feb. 2015.
- [2] Y. Gao, R. Ma, Y. Wang, Q. Zhang, and C. Parini, "Stacked patch antenna with dual-polarization and low mutual coupling for massive MIMO," *IEEE Trans. Antennas Propag.*, vol. 64, no. 10, pp. 4544–4549, Oct. 2016.
- [3] M. V. Komandla, G. Mishra, and S. K. Sharma, "Investigations on dual slant polarized cavity-backed massive MIMO antenna panel with beam-forming," *IEEE Trans. Antennas Propag.*, vol. 65, no. 12, pp. 6794–6799, Dec. 2017.
- [4] H. Huang, X. Li, and Y. Liu, "A low-profile, dual-polarized patch antenna for 5G MIMO application," *IEEE Trans. Antennas Propag.*, vol. 67, no. 2, pp. 1275–1279, Feb. 2019.
- [5] X. Chen, S. Zhang, and Q. Li, "A review of mutual coupling in MIMO systems," *IEEE Access*, vol. 6, pp. 24706–24719, 2018.
- [6] X. Yang, Y. Liu, Y.-X. Xu, and S.-X. Gong, "Isolation enhancement in patch antenna array with fractal UC-EBG structure and cross slot," *IEEE Antennas Wireless Propag. Lett.*, vol. 16, pp. 2175–2178, 2017.
- [7] S.-C. Chen, Y.-S. Wang, and S.-J. Chung, "A decoupling technique for increasing the port isolation between two strongly coupled antennas," *IEEE Trans. Antennas Propag.*, vol. 56, no. 12, pp. 3650–3658, Dec. 2008.
- [8] B. L. Dhevi, K. S. Vishvakshnan, and K. Rajakani, "Isolation enhancement in dual-band microstrip antenna array using asymmetric loop resonator," *IEEE Antennas Wireless Propag. Lett.*, vol. 17, no. 2, pp. 238–241, Feb. 2018.
- [9] H. Wong, K. Lau, and K. Luk, "Design of dual-polarized 1-probe patch antenna arrays with high isolation," *IEEE Trans. Antennas Propag.*, vol. 52, no. 1, pp. 45–52, Jan. 2004.
- [10] H. Zhai, L. Xi, Y. Zang, and L. Li, "A low-profile dual-polarized high-isolation MIMO antenna arrays for wideband base-station applications," *IEEE Trans. Antennas Propag.*, vol. 66, no. 1, pp. 191–202, Jan. 2018.
- [11] C. Wang, Y. Chen, and S. Yang, "Dual-band dual-polarized antenna array with flat-top and sharp cutoff radiation patterns for 2G/3G/LTE cellular bands," *IEEE Trans. Antennas Propag.*, vol. 66, no. 11, pp. 5907–5917, Nov. 2018.
- [12] J. Li, S. Yang, Y. Gou, J. Hu, and Z. Nie, "Wideband dual-polarized magnetically coupled patch antenna array with high port isolation," *IEEE Trans. Antennas Propag.*, vol. 64, no. 1, pp. 117–125, Jan. 2016.
- [13] B. C. Pan, "Reduction of the spatially mutual coupling between dual-polarized patch antennas using coupled metamaterial slabs," *Sci. Rep.*, vol. 6, Jul. 2016, Art. no. 30288.
- [14] M.-C. Tang, Z. Chen, H. Wang, M. Li, B. Luo, J. Wang, Z. Shi, and R. W. Ziolkowski, "Mutual coupling reduction using meta-structures for wideband, dual-polarized, and high-density patch arrays," *IEEE Trans. Antennas Propag.*, vol. 65, no. 8, pp. 3986–3998, Aug. 2017.
- [15] K.-L. Wu, C. Wei, X. Mei, and Z.-Y. Zhang, "Array-antenna decoupling surfaces," *IEEE Trans. Antennas Propag.*, vol. 65, no. 12, pp. 6728–6738, Dec. 2017.
- [16] E. Hassani, D. Noreland, R. Augustine, E. Wadbro, and M. Berggren, "Topology optimization of planar antennas for wideband near-field coupling," *IEEE Trans. Antennas Propag.*, vol. 63, no. 9, pp. 4208–4213, Sep. 2015.
- [17] L. Wang, G. Wang, and J. Sidén, "Design of fragment-type isolation structures for MIMO antennas," *Prog. Electromagn. Res. C*, vol. 52, pp. 71–82, 2014.
- [18] D. Lu, L. Wang, E. Yang, and G. Wang, "Design of high-isolation wideband dual-polarized compact MIMO antennas with multiobjective optimization," *IEEE Trans. Antennas Propag.*, vol. 66, no. 3, pp. 1522–1527, Mar. 2018.

- [19] Y.-F. Cheng, X. Ding, W. Shao, and B.-Z. Wang, "Reduction of mutual coupling between patch antennas using a polarization-conversion isolator," *IEEE Antennas Wireless Propag. Lett.*, vol. 16, pp. 1257–1260, 2017.
- [20] S.-H. Zhu, X.-S. Yang, J. Wang, and B.-Z. Wang, "Design of MIMO antenna structure based on a hybrid topology optimization method," *IEEE Trans. Antennas Propag.*, vol. 67, no. 10, pp. 6298–6307, Oct. 2019.
- [21] J. Wang, X.-S. Yang, X. Ding, and B.-Z. Wang, "Antenna radiation characteristics optimization by a hybrid topological method," *IEEE Trans. Antennas Propag.*, vol. 65, no. 6, pp. 2843–2854, Jun. 2017.
- [22] J. Wang, X.-S. Yang, X. Ding, and B.-Z. Wang, "Topology optimization of conical-beam antennas exploiting rotational symmetry," *IEEE Trans. Antennas Propag.*, vol. 66, no. 5, pp. 2254–2261, May 2018.
- [23] S. Zargham, T. A. Ward, R. Ramli, and I. A. Badruddin, "Topology optimization: A review for structural designs under vibration problems," *Struct. Multidisciplinary Optim.*, vol. 53, no. 6, pp. 1157–1177, Jun. 2016.
- [24] W. L. Stutzman and G. A. Thiele, *Antenna Theory and Design*, 3rd ed. Hoboken, NJ, USA: Wiley, 2012, pp. 466–477.



SHUN-HUI ZHU was born in Hunan, China, in 1992. He received the B.S. degree in electronic information science and technology from Southwest Petroleum University (SWPU), Chengdu, China, in 2015. He is currently pursuing the Ph.D. degree in radio physics with the University of Electronic Science and Technology of China (UESTC), Chengdu.

His research interests include computational electromagnetics, topology optimization methods, and MIMO antennas optimization and decoupling.



XUE-SONG YANG (Member, IEEE) received the B.Eng. degree in applied electronic technology from the Huazhong University of Science and Technology (HUST), Wuhan, China, in 1991, and the Ph.D. degree in radio physics from the University of Electronic Science and Technology of China (UESTC), Chengdu, China, in 2006.

She joined UESTC in 2002, where she is currently a Full Professor. From January 2007 to July 2008, she was a Senior Research Associate and then a Research Fellow with the City University of Hong Kong (CITYU). From December 2009 to December 2010, she was a Visiting Scholar with the University of Southern California (USC), USA. From July to August 2014, she was a Visiting Associate Professor with the City University of Hong Kong (CITYU). From December 2017 to December 2018, she was a Visiting Scholar with the National University of Singapore (NUS). Her current research interests include MIMO antennas, reconfigurable antennas, metasurface antennas, wireless energy transmission, and wireless communications channel modeling.



JIAN WANG was born in Hebei, China, in 1986. He received the B.S. and M.S. degrees and the Ph.D. degree in radio physics from the University of Electronic Science and Technology of China (UESTC), Chengdu, China, in 2009, 2012, and 2018, respectively.

He is currently a RF Engineer with The 13th Research Institute of China Electronics Technology Group Corporation (CETC), Shijiazhuang, China.



NIAN-SHENG NIE was born in Yunnan, China, 1994. He received the B.S. degree in electronic information science and technology from the University of Electronic Science and Technology of China (UESTC), Chengdu, China, in 2017, where he is currently pursuing the M.S. degree in radio physics.

His current research interests include antenna theory and engineering, phased arrays, and metasurface antennas.



BING-ZHONG WANG (Senior Member, IEEE) received the Ph.D. degree in electronic engineering from the University of Electronic Science and Technology of China (UESTC), Chengdu, China, in 1988.

He joined the UESTC in 1984, where he is currently a Professor. He has been a Visiting Scholar with the University of Wisconsin-Milwaukee, WI, USA, a Research Fellow with the City University of Hong Kong, Hong Kong, and a Visiting Professor with the Electromagnetic Communication Laboratory, Pennsylvania State University, University Park, PA, USA. His current research interests are in the areas of computational electromagnetics, antenna theory and technique, and time-reversed electromagnetics.

...